Fortgeschrittenenpraktikum

Tom Heinrich, Daniela Rolf, Guido Falk von Rudorff Asaf Avnon (Tutor)

25.01.2012 (Versuch), 02.02.2012 (Auswertung)

1 Gammaspektrometrie

basic information

Since gamma radiation has to be measured by observing different effects of interaction between matter and radiation the effect's basic principles are important for this experiment, that deals both with measurement of gamma radiation in general and two detector types in particular.

gamma spectra In this experiment gamma spectra of radioactive nuclides are the main topic. The gathered data helps to analyse the nucleus' states, the interaction of gamma rays and matter as well as the →detectors capabilities.

The spectras quality depends mainly on the detector that has been used in order to measure the data. In the best case with low noise background there are a few peaks that can be detected. The first ones are the photopeaks which are – within the measurements of this experiment – the result of beta →decays that emit photons. If these photons with an energy E_γ hit an electron with the binding energy $E_B \ll E_\gamma$ the electron will be detached from the nucleus and carry the kinetic energy E_m

$$E_m = E_\gamma - E_B = hf - E_B \tag{1.1}$$

E_B is typically in the order of a few electron volts. Although the energy E_m is less than E_γ, the recombination at the dynodes within the photomultiplier leads to a measurement of the full energy. The position with a lower energy level E_l that has been left empty will be filled by an electron from a higher energy level E_h. This can be achieved by emission of radiation which leads to K_α and K_β peaks at

$$E_\alpha = E_h - E_l \tag{1.2}$$

for different E_h. E_l corresponds to the ground state. Usually these states are degenerated, but the difference between the energy levels is far to small to be measured with the equipment used in this experiment. The second possibility is the emission of AUGER electrons that carry the energy

$$E_{ag} = E_\alpha - E'_B - E_B \tag{1.3}$$

Due to the fact that the AUGER process involves three electrons of which two are leaving the atom, two binding energies E_B and E'_B have to be subtracted. First the incoming photon detaches one electron. The second electron changes the energy level to that of the first one and emits a photon that detaches a third electron. The first electron is usually in one of the lowermost states.

Other peaks – one per photopeak – occur due to the COMPTON effect. The COMPTON effect is one possible interaction of gamma rays with matter. The photon will be scattered by a degree φ and the electron gets some kinetic energy from the photon and changes its direction. Due to energy conservation the photon's wavelength increases. The amount of energy T transferred from the photon to the electron depends on φ.

$$T = E_\gamma \left(1 - \frac{1}{1 + \frac{E_\gamma}{m_e c^2}(1 - \cos\varphi)} \right) \tag{1.4}$$

where E_γ is the energy of the photon before scattering. This formula can be obtained from the result of combining energy and momentum conservation

$$\lambda'_\gamma - \lambda_\gamma = \frac{h}{m_e c}(1 - \cos\varphi) \tag{1.5}$$

The COMPTON peak results from the maximum energy $T_{\max}$ for $\varphi = \pi$

$$T_{\max} = E_\gamma \left(1 - \frac{1}{1 + \frac{2E_\gamma}{m_0 c^2}} \right) \tag{1.6}$$

It is possible for a scattered photon to leave the detector – in this case the measured energy for this decay is too low.

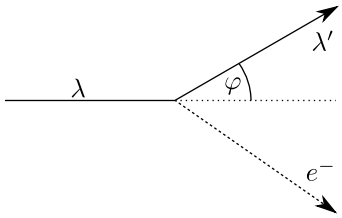

Fig. 1.1: geometry of COMPTON scattering of a photon with the wavelengh λ before and λ' after the scattering with the electron e^- and the angle φ

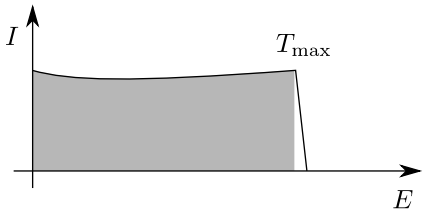

Fig. 1.2: the COMPTON spectrum until $T_{\max}$; cf. [7]

Another possibility is the occurrence of scattering outside the detector. The result is the so called backscatter peak at

$$E_{bs} = E_\gamma - T_{\max} \tag{1.7}$$

Another type of peaks are the escape peaks. In case the photon carries more than twice the rest energy of an electron, pair production is possible. The result of this process is one electron and one positron that will annihilate with another electron and emits two photons with the rest energy of an electron (511 keV). If one of this photons escapes the detector, the peak is called single-escape peak;

if both photons escape the detector, it is called double-escape peak. For each photopeak E_x with an energy of more than 1022 keV the escape peaks should occur at

$$E_s = E_x - m_e c^2 \qquad E_d = E_x - 2m_e c^2 \tag{1.8}$$

This process is possible outside the detector as well. In this case one of the photons can reach the detector which leads to an annihilation peak at

$$E_{an} = m_e c^2 \simeq 511 \text{ keV} \tag{1.9}$$

decay Although there are three main types of decay the most important in this experiment – cf. Tab. (1.1) – is the beta decay that follows

$${}^1_0\text{n} \rightarrow {}^1_1\text{p} + \text{e}^- + \overline{\nu}_e \tag{1.10}$$

for the β^- decay and

$${}^1_1\text{p} \rightarrow {}^1_0\text{n} + \text{e}^+ + \nu_e \tag{1.11}$$

for the β^+ decay. The daughter nuclei are mostly in an excited state. The positron resulting from β^+ decay annihilates within the detector or at least nearby so the intensity of the annihilation line is much higher than expected, especially since the annihilation leads to two 511 keV photons due to conservation of momentum.

nuclide	decay	result	energy [keV]
${}^{22}_{11}$Na	β^+	${}^{22}_{10}$Ne (stable)	1274,5
${}^{60}_{27}$Co	β^-	${}^{60}_{28}$Ni (stable)	1173,2; 1332,5
${}^{137}_{55}$Cs	β^-	${}^{137}_{56}$Ba (stable)	661,7
${}^{133}_{56}$Ba	β^+	${}^{133}_{55}$Cs (stable)	31,0; 81,0; 356,0
${}^{241}_{95}$Am	α	${}^{237}_{93}$Np (α)	13,9; 59,5

Tab. 1.1: nuclides used in this experiment, their main decay type, the daughter nuclei and the most important photopeaks according to [1]

The process of alpha decay can be described as

$${}^A_Z\text{X} \rightarrow {}^{A-4}_{Z-2}\text{Y} + {}^4_2\text{He} \tag{1.12}$$

If the nucleus is in an excited state it is possible that the energy difference to the ground state is directly emitted by an electron. This process is similar to the AUGER process but involves only one electron.

$${}^A_Z\text{X}^* \rightarrow {}^A_Z\text{X} + \text{e}^- \tag{1.13}$$

This effect is called internal conversion.

detector γ radiation is detected using indirect methods. In this experiment two kinds of detectors are used: a NaJ(Tl) scintillation counter and a germanium detector.

The scintillation counter consists of a crystal that is sensitive to photons with an energy of the radiation being analysed and reacts with fluorescence to incoming photons. The resulting photons carry less energy than the first ones, but detach electrons from the side of the crystal that is covered by a photomultiplier due to photo effect. The other sides of the crystal are covered in order to reflect the radiation. The photomultiplier rises the current by a factor of 10^6 to 10^{10}. This way even single photons can be detected. The resolution of this kind of detector is about 6-10% and the dead time in the order of 10^{-6}s[12, 4].

The germanium detector can be thought of as a diode with a voltage in reverse direction. An incoming photon creates electron-hole pairs whose amount is linear proportional to the energy of the photon – on average one pair per 2.98 eV. Since the voltage will „remove“ the electron-hole pairs from the active germanium zone, a current can be measured. In order to assure the necessary sensitivity a small amount of lithium is added to the active material.[5] For bigger detectors it is complicated to obtain the demanded concentration so permanent cooling to a temperature like -20°C for storage is necessary[4]. During the whole experiment the temperature must not exceed -196°C in order to keep the noise, the reverse current, low enough [4] – this is archieved by the use of liquid nitrogen. The energy resolution of a semiconductor based detector is [5] about 0.15%. The dead time of a semiconductor based detector is [4] in the order of 10^{-6}s.

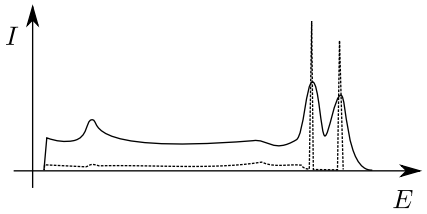

Fig. 1.3: schematic comparison concerning the resolution of the scintillation counter (stroked) and the germanium detector (dashed) for a ^{60}Co source according to [9]

The signals of both types of detectors are – after two chained amplifiers applied some corrections – proportional to the energy of the photons from the radiation, since both the work function and the middle energy necessary to create an electron-hole pair is constant and with few eV relatively small compared to the energy of the photon that ranges from few keV to few MeV. The amplifiers change the parameter to be measured as well: the detectors' output is a current, the filter's output is a voltage. A multichannel analyser sorts and counts these impulses. The calibration between channel and energy can be done using at least two sources emitting radiation of known energy, since of the linearity of the correlation [5].

Another property both detectors have in common is the width of the peaks: although the germanium detector has sharper peaks neither the scintillation counter nor the semiconductor detectors lead to discrete values. From the statistical point of view a gauss distribution with

$$\sigma^2 = N \tag{1.14}$$

would be expected. Experimental data shows that this edge case is a far to pessimistic approximation. Therefore

the FANO factor F is introduced[6]

$$\sigma^2 = FN \qquad 0 < F \leq 1 \tag{1.15}$$

A typical value [4] for F concerning data gathered using a semiconductor detector is 0.1-0.2, the detector in this experiment has [5] a fano factor of approximately 01.. For scintillation counters [9] the FANO factor is $\simeq 1$. The energy resolution R depends on the FANO factor

$$R = 2,35\frac{\sqrt{FN}}{N} \tag{1.16}$$

with the amount of events N. So a lower FANO factor leads to a better energy resolution.

mass attenuation coefficient The attenuation of gamma radiation within matter depends on the material's thickness x and follows

$$I(x) = I_0 e^{-\mu x} \tag{1.17}$$

where I_0 is the intensity at $x = 0$ and μ is the attenuation coefficient. μ/ρ is the mass attenuation coefficient. μ can be obtained [9] from the density of atoms N of the material being used and the cross section σ'

$$\mu = N\sigma' = \sigma'\frac{N_A\rho}{m} \tag{1.18}$$

where N_A is AVOGADRO's Number, ρ the density and m the molecular weight. The value of σ' depends on separate cross sections from the possible interaction processes. Assuming that only electrons from the K shell are involved in the photo effect the dependence on the atomic number Z of the photo effect cross section σ_P can be estimated[9] to

$$\sigma_P \propto \frac{Z^4}{E^3} \tag{1.19}$$

The exact value for the exponent depends on the energy of the radiation – in general higher energy leads to lower cross section. One exception is important and will be used for the measurement of the conversion energy: if the energy of radiation is a little bit smaller than the binding energy of a shell the cross section drops significantly. This peak is named after the shell being involved – in this experiment the K edge will be analysed. The binding energy of the K shell depends on the atomic number Z. This relation can be approximated[12] for K shell electrons

$$E_B \simeq E_0(Z-1)^2 \tag{1.20}$$

with the binding energy of the hydrogen atom E_0. Using absorbers with a different Z the K edge can be shifted along the energy axis.

Two other cross sections are important. The first one belongs to COMPTON scattering and scales[2] with regard to all Z electrons

$$\sigma_C \propto \frac{Z}{E} \tag{1.21}$$

and the second one belonging to pair production[12]

$$\sigma_{PP} \propto Z^2 \ln E \tag{1.22}$$

The total cross section necessary to obtain μ is given by

$$\sigma' = \sigma_P + \sigma_C + \sigma_{PP} \tag{1.23}$$

Fig. (1.4) shows that one these three cross sections is big enough for every wavelength to be absorbed. If the detector is big enough every radiation that is not being reflected out of the detector will be registered.

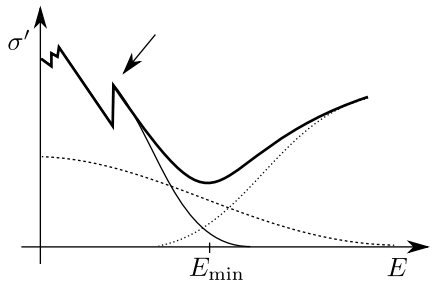

Fig. 1.4: dependence of σ' (stroked, bold) on the photon's energy according to [9, 2] with σ_P (stroked, thin), σ_C (dashed), σ_{PP} (dotted) and the K edge (arrow). $E_{\min}$ depends on the material used for the experiment and its typical value is about 5 MeV. The energy axis is scaled logarithmically.

experimental setup

The radioactive material was placed behind a shield of lead and was kept there as long as possible. In order to reduce the radiation dose as much as possible all repositioning of the different isotopes has been performed by the help of tweezers. The cooling necessary for the germanium detector and the settings for the scintillation counter was prepared by the tutor.

The ^{60}Co sample with a higher intensity was placed in an additional cylindric shield. The other samples were fixed within a small disc made of plastic that could be attached to a lead brick holding the disc for the duration of the experiment.

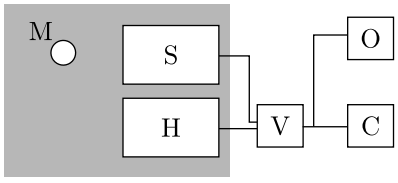

Fig. 1.5: the setup for measurement with radioactive material M, the scintillation counter S and the germanium detector H on the table (grey), the amplifier V, the oscilloscope O and the computer C

tasks

scintillation counter

With the ^{137}Cs sample mounted the oscilloscope was used to determine the effect of the amplifier. The amplifier allowed to change the gain and a time constant. First of all we adjusted the settings to obtain a clearer image from the oscilloscope. Then the oscilloscope's cursor function has been used to measure the rise and fall time of the signal before and after the amplifier. The datasets in fig. (1.6) and (1.7) whose errors has been estimated to 0.5 μs and 0.05 V had to be separated into two diagrams due to their different voltage level.

Unfortunately the oscilloscope could not display the very first 2 μs of the signal. We guess that this behaviour is related to the trigger signal, but changing the trigger level did not resolve this problem. Therefore the rise time before the amplifier can only be estimated to

$$t_r = (2 \pm 0.5)\,\mu\text{s}$$

The error of t_r is estimated as well and corresponds to the error of the measured data. Linear regression applied to the data in the range of 2-15 μs leads to the fall time. The linear function

$$f_f(t) = a_f t - b_f$$

with

$$a_f = (0.0516 \pm 0.0025)\frac{\text{V}}{\mu\text{s}}$$

$$b_f = (-1.241 \pm 0.023)\text{V}$$

is plotted in fig. (1.6). The intersection of the regression line and the x axis determines the fall time t_f but t_r has to be subtracted.

$$t_f = \frac{-b_f}{a_f} - t_r \tag{1.24}$$

The gaussian error propagation gives

$$\Delta t_f = \sqrt{\frac{b_f^2}{a_f^4}(\Delta a_f)^2 + \frac{1}{a_f^2}(\Delta b_f)^2 + (\Delta t_r)^2} \tag{1.25}$$

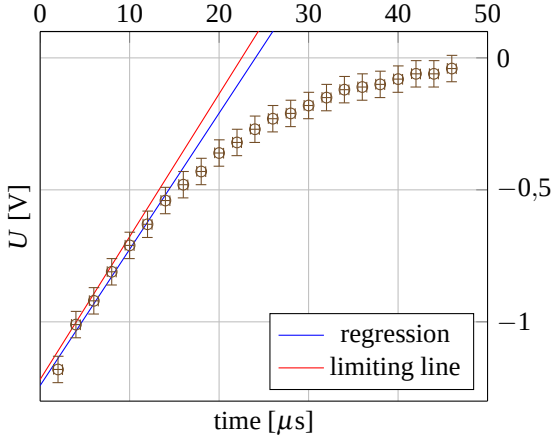

Fig. 1.6: voltage over time before the amplifier

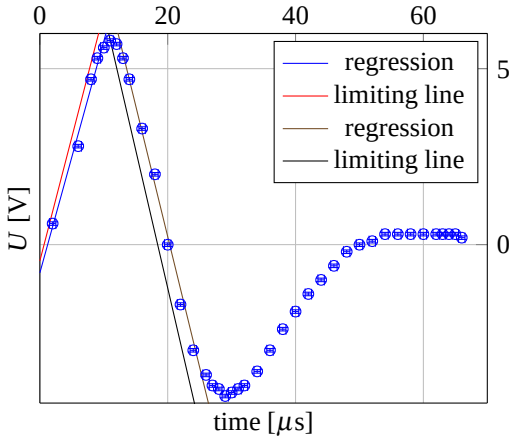

Fig. 1.7: voltage over time after the amplifier; the error bars are very small

and therefore

$$t_f = (24.1 \pm 1.3)\,\mu\text{s}$$

The same procedure can be applied to the other measured datasets. First of all the beginning of the sine shaped curve has to be determined. Linear regression on

$$f_r'(t) = a_r' t - b_r'$$

applied to the four first datapoints of fig. (1.7) leads to

$$a_r' = (0.658 \pm 0.045)\frac{\text{V}}{\mu\text{s}}$$

$$b_r' = (-0.80 \pm 0.34)\text{V}$$

The maximum t_m of the sine shaped curve is at

$$t_m = (12 \pm 0.5)\,\mu\text{s}$$

So the rise time t_r' can be calculated

$$t_r' = t_m + \frac{b_r'}{a_r'} \tag{1.26}$$

with

$$\Delta t_r' = \sqrt{\frac{b_r'^2}{a_f^4}(\Delta a'_r)^2 + \frac{1}{a_r'^2}(\Delta b'_r)^2 + (\Delta t_r')^2} \tag{1.27}$$

$$t_r' = (10.78 \pm 0.72)\,\mu\text{s}$$

Using a third linear regression for the data between 13 and 20 μs the fall time t_f' with

$$f_f'(t) = a_f' t - b_f'$$

and

$$a_f' = (-0.743 \pm 0.040)\frac{\text{V}}{\mu\text{s}}$$

$$b'_f = (15.09 \pm 0.66)\text{V}$$

gives

$$t'_f = (9.5 \pm 1.5)\,\mu\text{s}$$

with

$$t'_f = \frac{-b'_f}{a'_f} - t_m \tag{1.28}$$

and the error calculated by the gaussian error propagation – as it will be done throughout the entire protocol.

The most important observation is the reduced fall time at the cost of an increased rise time. The sum of the rise and fall time remains approximately the same, but a sine shaped curve is much easier to analyse. The shape of the measured data before the amplifier corresponds to the physical processes involved: the fraction of relaxated atoms during the fluorescence follows an exponential curve and depends on the material being used so the fall time should be much longer than the rise time. According to [8] it might have been possible to resolve the peak before the amplifier by increasing the time constant setting, since that should scale the data from fig. (1.6) along the time axis. Unfortunately the setup did not allow to increase the time constant even more.

photopeaks: scintillation counter

For the second part of the experiment the gain and the time constant of the amplifier were changed in order to extend the spectrum to the full range of the multichannel analyser and maintain the peaks' shape. We used approximately 3000 channels. Choosing a wider range caused the measured data to be much less significant. The total number of events counted is about 879,000 for ^{60}Co, 224,000 for ^{22}Na and 306,000 for ^{137}Cs. For each measurement we waited until the relative shape of the peaks didn not change anymore.

Fig. (1.8) shows an example of the datapoints. The relevant data for each photopeak (position and FWHM) has been determined using the computer program MAESTRO and is listed in tab. (1.2). It has been helpful to know the relative positions of the photopeaks since the ^{22}Na measurement's highest peak is not a photopeak.

The given energies of the photopeaks can be used to define the linear dependence between channel number and energy as shown in fig. (1.9).

peak	min	top	max	FWHM
^{60}Co: 1	1921	2012	2102	181
^{60}Co: 2	2156	2262	2324	168
^{22}Na	2077	2130	2173	96
^{137}Cs	1192	1254	1311	119

Tab. 1.2: measured data for different photopeaks with the peak at channel „top“, and the boundaries relevant to the FWHM „min“ and „max“; all data specified in channels

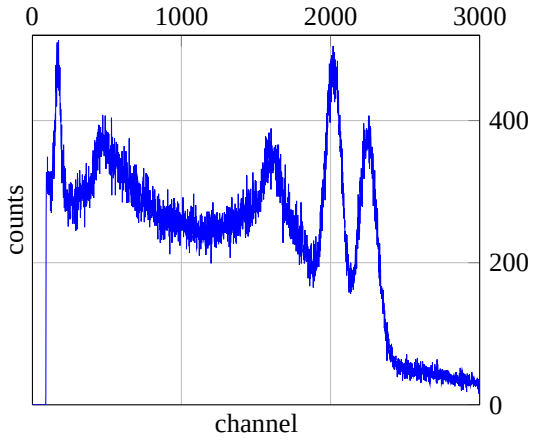

Fig. 1.8: recorded spectrum for ^{60}Co as an example; only the lowermost 3000 channels are visible; the other spectra show similar shaped peaks

With the channel number α the energy in keV $E(\alpha)$ is

$$E = c\alpha + d \tag{1.29}$$

with

$$c = (0.677 \pm 0.021)\text{ keV}$$

$$d = (186 \pm 40)\text{ keV}$$

This relation is plotted in fig. (1.9) as well and necessary to calculate the energy resolution δ in tab. (1.3).

$$\delta = \frac{\Delta E}{E} \tag{1.30}$$

where ΔE equals the half FWHM.

The results seem to be reasonable as the energy resolution should be in the order of a few percent[4]. The coefficient of determination

$$R^2 = 0.998$$

confirms the expected linear dependence.

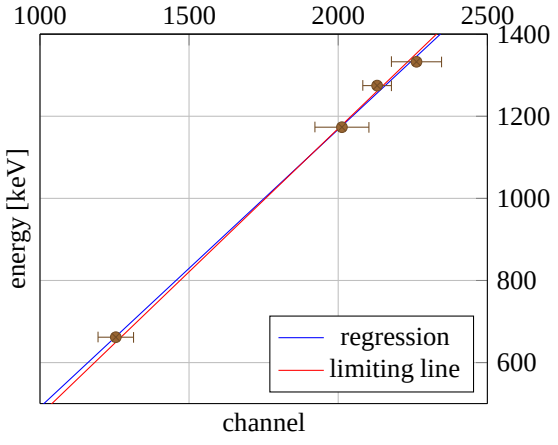

Fig. 1.9: measured positions of the photopeaks and their energies

peak	energy [keV]	δ
^{60}Co: 1	(1176 ± 61)	0,05
^{60}Co: 2	(1345 ± 57)	0,04
^{22}Na	(1256 ± 33)	0,03
^{137}Cs	(662 ± 40)	0,06

Tab. 1.3: Calculated data for different photopeaks with the energy resolution δ. All the values agree with the reference values in tab. (1.1) – the correlation is much better than the calculated errors.

mass attenuation coefficient

For each of the materials lead, copper and aluminium a set of plates was given. The plates' thickness was in the range of two to four millimetres. Various combinations of those plates were used to measure the dependence of intensity on the thickness. The plates were clamped vertically between two bricks of lead so the radiation of a ^{60}Co source passed through this shield and reached the scintillation detector. Due to the high intensity of radiation the source was shielded itself within a cylindric box made of lead.

MAESTRO, the software that has been used to calculate the information, allows the user to specify a region of interest and computes the total count rate by integrating the counts „gross area“ and the noise that has to be subtracted. In the software's terminology this area is called „net area“. In order to compare the count rates the duration of the measurement had to be constant. We first tried a thick layer of lead and waited until the spectrum seemed to be mostly stable. This took approximately two minutes, so the further measurements were timed to this duration using a stopwatch. The time error can be estimated to half a second. That's rather short but reasonable for a expected event. The use of the internal stopwatch of MAESTRO would be an alternative. The highest total count rate during the two minutes was registered for no shielding at all and is about N =83,000 so the average count rate measured during the time error is 346 and the statistical error $\sqrt{N}$ is 288. These two errors have to be combined in order to analyse the data

$$\Delta N = \sqrt{N} + \frac{N}{240} \tag{1.31}$$

The dead time of a scintillation counter is in the order of 10^{-6} which gives the limit of 1,000,000 events per second. The highest number occurred here is 692 events per second. That confirms the choice of placing the strong ^{60}Co source approximately 10cm away from the scintillation detector. The gap could be narrowed in the case a tripod or similar equipment to hold the plates would have been available.

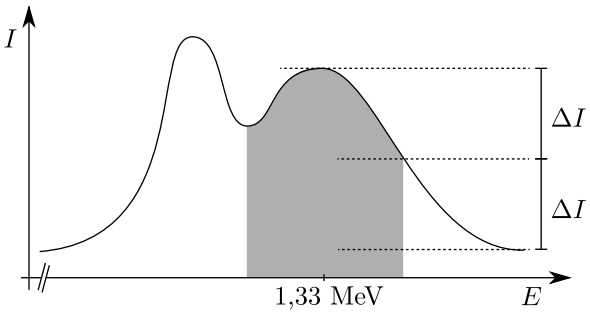

Fig. 1.10: a simplified shape of the two ^{60}Co photopeaks with the (grey) range used to obtain the „gross area“ and „net area“

material	thickness [mm]	gross area	net area	total count rate	ln(total count rate)
–	0	(82600 ± 630)	(12720 ± 170)	(69880 ± 650)	(11.1545 ± 0.0093)
lead	$(2{,}0 \pm 0{,}1)$	(78250 ± 610)	(8600 ± 130)	(69650 ± 620)	(11.1512 ± 0.0089)
lead	$(3{,}0 \pm 0{,}1)$	(76350 ± 590)	(11920 ± 160)	(64430 ± 620)	(11.073 ± 0.010)
lead	$(5{,}5 \pm 0{,}1)$	(60160 ± 500)	(12050 ± 160)	(48110 ± 520)	(10.781 ± 0.011)
lead	$(8{,}0 \pm 0{,}1)$	(53550 ± 460)	(10600 ± 150)	(42950 ± 480)	(10.668 ± 0.011)
lead	$(12{,}0 \pm 0{,}1)$	(43100 ± 390)	(6940 ± 110)	(36160 ± 400)	(10.496 ± 0.011)
copper	$(3{,}0 \pm 0{,}1)$	(74870 ± 590)	(8270 ± 130)	(66600 ± 600)	(11.1064 ± 0.0090)
copper	$(6{,}0 \pm 0{,}1)$	(69030 ± 550)	(10370 ± 150)	(58660 ± 570)	(10.980 ± 0.010)
copper	$(9{,}0 \pm 0{,}1)$	(63290 ± 520)	(8610 ± 130)	(54680 ± 530)	(10.909 ± 0.010)
copper	$(11{,}0 \pm 0{,}1)$	(54920 ± 460)	(6470 ± 110)	(48460 ± 480)	(10.788 ± 0.010)
copper	$(12{,}0 \pm 0{,}1)$	(52380 ± 450)	(9660 ± 140)	(42720 ± 470)	(10.662 ± 0.011)
aluminium	$(3{,}0 \pm 0{,}1)$	(71310 ± 560)	(9230 ± 130)	(62080 ± 580)	(11.0362 ± 0.0093)
aluminium	$(6{,}0 \pm 0{,}1)$	(71250 ± 560)	(9790 ± 140)	(61460 ± 580)	(11.0262 ± 0.0095)
aluminium	$(9{,}0 \pm 0{,}1)$	(64890 ± 530)	(7210 ± 120)	(57680 ± 540)	(10.9627 ± 0.0093)
aluminium	$(12{,}0 \pm 0{,}1)$	(61450 ± 500)	(7130 ± 110)	(54320 ± 520)	(10.9026 ± 0.0095)
aluminium	$(15{,}0 \pm 0{,}1)$	(59800 ± 490)	(10100 ± 140)	(49700 ± 510)	(10.814 ± 0.010)

Tab. 1.4: measured and calculated data for the different count rates during a data capture of two minutes. Only gross and net area are measured values.

Fig. (1.10) shows the range we decided to analyse with the software for each measurement. The left limit is the minimum between the two photopeaks and the right one the position where the count rate is reduced to half the maximum disregarding the noise. The results depended strongly on the defined region.

The thickness of the plates was given by labels attached to them specifying the value in 1/10 mm. The error was therefore estimated to 1/10 mm and reflects the error resulting from positioning the plates at different angles as well.

During the ongoing measurements the data from tab. (1.4) was plotted. With the absorber's thickness d the logarithmic value of the count rate can be analysed

$$\Delta(\ln N) = \sqrt{\left(\frac{\partial \ln N}{\partial N}\right)^2 (\Delta N)^2} = \frac{\Delta N}{N} \tag{1.32}$$

The results of the linear regression on

$$g(x) = -\mu d + b \tag{1.33}$$

with the depth d and the intercept b is given in tab. (1.5). b equals the natural logarithm of the intensity in the border case without any shielding and should be identical. Considering the error ranges this condition is met.

Given the densities ρ the mass attenuation coefficient

$$\mu_P = \frac{\mu}{\rho} \tag{1.34}$$

can be obtained.

Tab. (1.6) shows the results together with the reference values. The results for lead are identical within the error range, the other two are compatible with the reference data. The results meet the expectations as well: lead is much more efficient as shielding in terms of thickness, and aluminium is approximately as usable for shielding as lead with regard to the necessary mass.

mat.	μ [1/cm]	b	R^2
Pb	(0.619 ± 0.072)	(11.202 ± 0.047)	0.95
Cu	(0.386 ± 0.051)	(11.197 ± 0.041)	0.93
Al	(0.207 ± 0.020)	(11.138 ± 0.018)	0.96

Tab. 1.5: calculated values for the attenuation coefficient μ for differerent materials using linear regression with coefficient of determination R^2

mat.	ρ [g/cm^3]	μ_P [cm^2/g]	μ_P^* [cm^2/g]
Pb	11.34	(0.055 ± 0.006)	0.059
Cu	8.96	(0.043 ± 0.006)	0.053
Al	2.7	(0.076 ± 0.007)	0.055

Tab. 1.6: calculated values for the mass attenuation coefficient μ_P for differerent materials with their densities ρ according to [3] and the reference value μ_P^* [10] for a energy of 1.25 MeV

The dominant effect in this energy range is COMPTON scattering[9]. The coarse gain setting was set to 20, the time constant to 8 μs and the fine gain to 0.7.

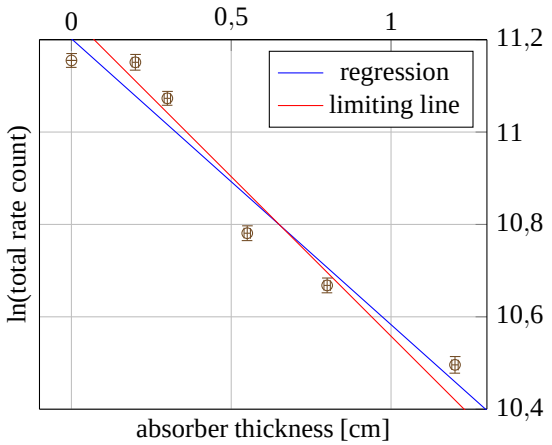

Fig. 1.11: decreasing intensity of radiation for the 1.33 MeV photopeak of ^{60}Co and lead shielding

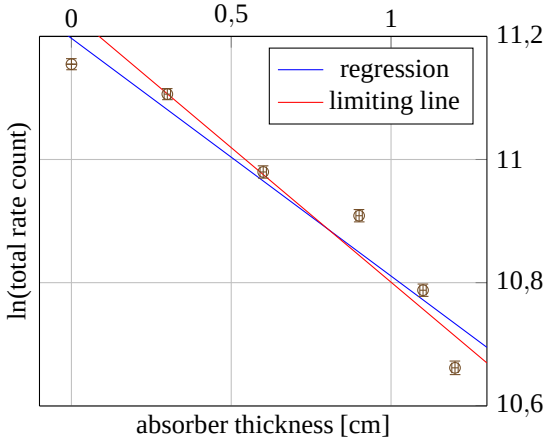

Fig. 1.12: decreasing intensity of radiation for the 1.33 MeV photopeak of ^{60}Co and copper shielding

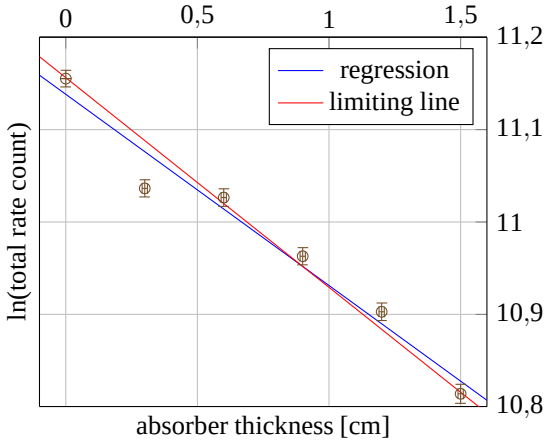

Fig. 1.13: decreasing intensity of radiation for the 1.33 MeV photopeak of ^{60}Co and aluminium shielding

germanium detector

Following the same procedure as in the first task the properties of the germanium detector should be determined. The only change necessary to the setup was to switch the cable between detector and amplifier. Afterwards the oscilloscope was used to record the shape necessary to measure rise and fall time. The coarse gain setting was set to 50, the time constant to 4 μs and the fine gain to 0.7. This way the curves shown by the oscilloscope were not stable but recordable. Due to this fluctuation the error had to be estimated higher than in the first task: 5mV and 5μs – that corresponds to 1/10 of a unit displayed by the oscilloscope.

The data in fig. (1.14) follows the expected shape – cf. the first task. The rise time before the amplifier was calculated by the intersection of the linear regression function

$$h(t) = i_r t + j_r \tag{1.35}$$

for the first three data points in fig. (1.14) with a constant function at the maximum of the peak $U_m = (165 \pm 5)$ mV.

$$i_r = (8.00 \pm 0.58)\frac{\text{mV}}{\mu\text{s}}$$

$$j_r = (-77 \pm 12)\ \text{mV}$$

give the rise time τ_r with respect to the offset $o_r = (10 \pm 5)\,\mu$s (the first measured datapoint)

$$\tau_r = \frac{U_m - j_r}{i_r} - o_r = (20.3 \pm 5.5)\mu\text{s}$$

with

$$\Delta\tau_r = \sqrt{\frac{(\Delta U_m)^2 + (\Delta j_r)^2}{i_r^2} + \frac{(U_m - j_r)^2}{i_r^4}(\Delta i_r)^2 + (\Delta o)^2} \tag{1.36}$$

Using the four datapoints after the maximum for linear regression gives

$$i_f = (-1.20 \pm 0.17)\frac{\text{mV}}{\mu\text{s}}$$

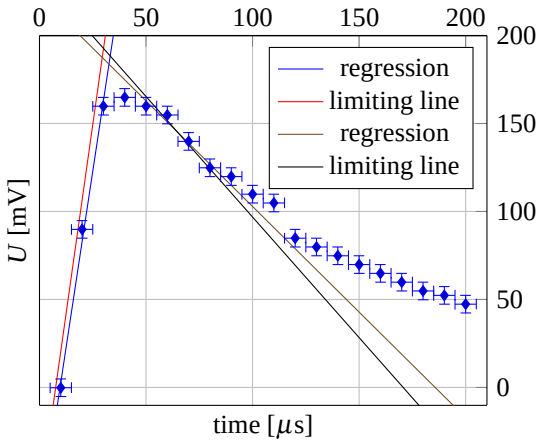

Fig. 1.14: voltage over time before the amplifier

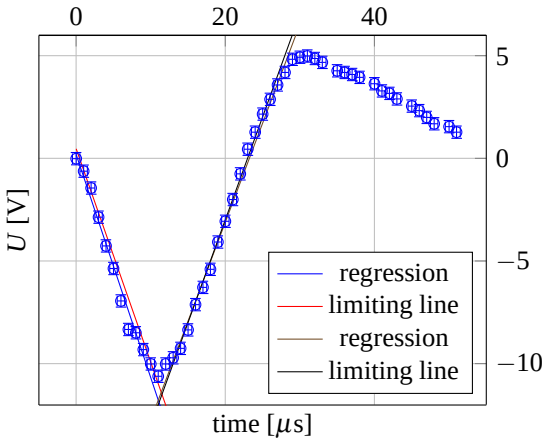

Fig. 1.15: voltage over time after the amplifier

$$j_f = (223 \pm 11)\ \text{mV}$$

which in turn lead to the fall time τ_f with the offset $o_f = (40 \pm 5)\,\mu$s (the peak's maximum)

$$\tau_f = \frac{-j_f}{i_f} - o_f = (146 \pm 28)\mu\text{s}$$

with

$$\Delta\tau_f = \sqrt{\frac{(\Delta j_f)^2}{i_f^2} + \frac{j_f^2(\Delta i_f)^2}{i_f^4} + (\Delta o_f)^2} \tag{1.37}$$

The recorded data for the peak after the amplifier is shown in fig. (1.15). The error has been estimated to 0.5 μs and 0.3 V.

Applying the same methods as mentionned above to this data with $U_m = (-10.6 \pm 0.3)$ V and $o_r' = 0$ gives

$$i_r' = (-1.087 \pm 0.047)\frac{\text{mV}}{\mu\text{s}}$$

$$j_r' = (0.20 \pm 0.28)\ \text{mV}$$

for the range between start and the maximum and therefore

$$\tau_r' = (9.94 \pm 0.57)\mu\text{s}$$

The result for the range between maximum and zero crossing with $o_f' = (11.0 \pm 0.5)\,\mu$s (the peak's minimum) is

$$i_f' = (0.964 \pm 0.038)\frac{\text{mV}}{\mu\text{s}}$$

$$j_f' = (-22.37 \pm 0.66)\ \text{mV}$$

and

$$\tau_f' = (12.2 \pm 1.2)\mu\text{s}$$

has been plotted in fig. (1.15).

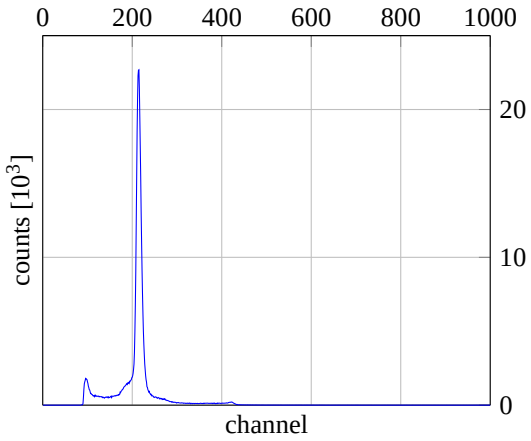

Fig. 1.16: recorded spectrum for ^{241}Am as an example; only the lowermost 1000 channels are visible; the other spectra show similar shaped peaks

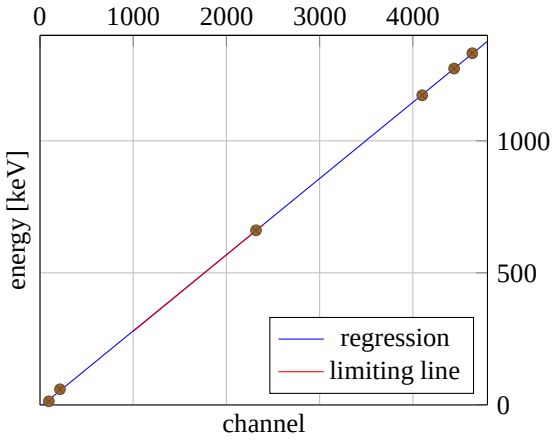

Fig. 1.17: measured positions of the photopeaks and their energies

peak	min	top	max	FWHM
^{60}Co: 1	4627	4632	4637	10
^{60}Co: 2	4095	4100	4104	9
^{22}Na	4434	4442	4446	12
^{137}Cs	2313	2317	2325	12
^{241}Am: 1	208	214	220	12
^{241}Am: 2	91	95	105	14

Tab. 1.7: measured data for different photopeaks with the peak at channel „top“, and the boundaries relevant to the FWHM „min“ and „max“; all values specified in channels

peak	energy [keV]	δ
^{60}Co: 1	$(1330{,}0 \pm 1{,}4)^*$	0,001
^{60}Co: 2	$(1175{,}7 \pm 1{,}3)^*$	0,001
^{22}Na	$(1274{,}5 \pm 1{,}7)^+$	0,001
^{137}Cs	$(661{,}0 \pm 1{,}7)^+$	0,003
^{241}Am: 1	$(53{,}8 \pm 1{,}7)^-$	0,03
^{241}Am: 2	$(19{,}5 \pm 2{,}0)^*$	0,10

Tab. 1.8: Calculated data for different photopeaks with the energy resolution δ. Values agree (*), disagree ($^-$) or are identical ($^+$) with the reference values in tab. (1.1). The reason for this behaviour is the very small error range.

peak	energy [keV]	β	β'
COMPTON: 1	1118,1	3730	3719
COMPTON: 2	963,4	3218	3209
backscatter: 1	214,4	740	738
backscatter: 2	209,8	725	723 (?)
single escape: 1	821,5	2749	2745
single escape: 2	662,2	2223	–
double escape: 1	310,5	1058	1041
double escape: 2	151,2	531	–
annihilation	511	1721	1707

Tab. 1.9: the possible peaks with their expected energy converted to a theoretical channel number β together with the measured channel number β'. The photopeaks are listed in tab. (1.8) and are not repeated. The backscatter peak for the second photopeak seems to be plausible but is not clearly distinguishable from the first photopeak's backscatter peak.

photopeaks: germanium detector

This task is basically the same as the second one: the main difference is the use of the germanium detector and the additional sample of ^{241}Am. Therefore the same nomenclature will be used and only methodical differences compared to task two are described.

This time the adjustment was easier so approximately 5000 channels could be used. A sample of the results is shown in fig. (1.16). The measurements have a total count rate of 464,000 (^{241}Am), 65,000 (^{22}Na), 229,000 (^{137}Cs) and 1,922,000 for ^{60}Co. In the first three cases we waited until the peaks seemed not to be sharpened anymore. In the last case we erroneously assumed that the weak source should be used for the detaillied spectrum analysis later on.

Again the peak's data was observed using the computer and is shown in tab. (1.7).

The linear regression for eqn. (1.29) leads to

$$c' = (0.28870 \pm 0.00092)\,\text{keV}$$

$$d' = (-7.9 \pm 3.0)\,\text{keV}$$

which in turn gives the data in tab. (1.8).

This time not only the energy resolution is much better and agrees with [9] in most cases; the coefficient of determination has increased

$$R'^2 = 0.99996$$

The values for ^{241}Am can not be compared to the former results for the scintillation counter directly since there were no measurements for energies this low.

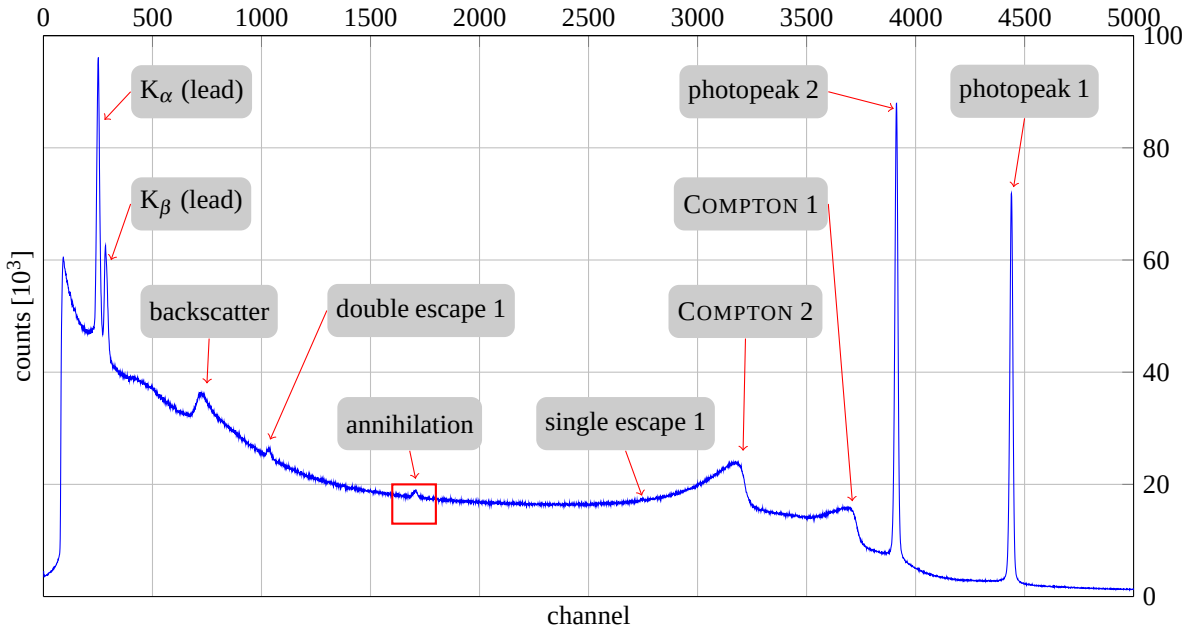

Fig. 1.18: detailled spectrum for ^{60}Co recorded using a long time exposure. The red box shows the magnified range in fig. (1.19)

The full spectrum of ^{60}Co recorded with the strong source for about 35 minutes is shown in fig. (1.18) and is based on about 94,077,000 events. Unfortunately the amplifier's settings had changed so the calibration in fig. (1.18) is different from the one in tab. (1.8).

$$E'' = 0,302 \text{ keV } \beta - 9,307 \text{ keV} \qquad (1.38)$$

with the channel number β.

The expected and found peaks are listed in tab. (1.9). In general the positions are near enough to be considered equal, but a constant offset of a few channels is evident. Considering the FWHM measured for the energy resolution a deviation of 5-10 channels can be estimated as error. In this case all visible peaks are at least compatible. The escape peaks for the second photopeak were not visible. Instead two new peaks arose around channel 258 and 291 (69 and 79 keV). Those are the K_α and K_β peaks of lead resulting from the shielding, which are found at 75 keV and 85 keV[11]. The differences between measured data and reference result from the less accurate calibration in combination with the measurement error. Two photopeaks are not reliable enough but a good approximation: within the spectrum recorded for the weaker ^{60}Co source these peaks are at approximately 69 and 80 keV. The comparison of the weak source's spectrum and the one of higher activity shows clearly how advantageous a higher count rate is with respect to statistical effects. Fig. (1.19) shows the fluctuation of both sources.

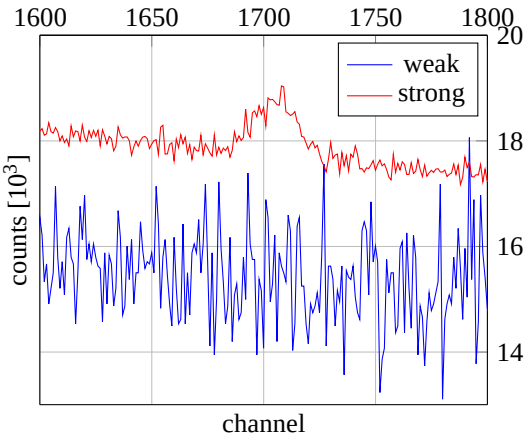

Fig. 1.19: fluctuation of the weak and strong ^{60}Co source near the annihilation peak that is missing within the data gained from the weak source. The weak source's data has been scaled by 42.

absorber	Z	reference gross	reference net	K_α gross	K_α net	φ
Sn	50	(22010 ± 150)	(15480 ± 120)	(7709 ± 87)	(2576 ± 50)	(0.79 ± 0.01)
Sb	51	(21110 ± 150)	(15860 ± 130)	(8331 ± 91)	(2185 ± 47)	(1.17 ± 0.02)
Te	52	(10730 ± 100)	(6796 ± 82)	(18160 ± 140)	(9580 ± 98)	(2.18 ± 0.03)
I	53	(19320 ± 140)	(13860 ± 120)	(29590 ± 170)	(19950 ± 140)	(1.76 ± 0.02)

Tab. 1.10: atomic number Z and count rates for the reference peak at 81 keV and the K_α peak [1] at 31 keV (both measured) with the calculated values φ

K_α line of ^{133}Ba

The last task was the measurement of the K_α line of ^{133}Ba. Perhaps „measurement“ is the wrong expression, since the range for the K edge can only be narrowed. The concept of this method is to use the significant drop of the cross section around the K edge – cf. fig. (1.4). In order to suppress disturbing effects from the positioning or the duration of the measurement the intensity of two peaks were compared for each spectrum. That's another approximation, since the reference peak at 81 keV is influenced by the absorber's K edge as well. Therefore the results are basically qualitative. The ratio between the K_α peak's count rate and the reference peak's is called φ in tab. (1.10).

With additional information [11] concerning the energy of the K_α transition the datapoints in fig. (1.20) could be calculated. The significant change of φ is evident – the K_α line of ^{133}Ba is between the inner two datapoints

$$K_\alpha = (30.4 \pm 0.6)\ \text{keV}$$

This value is confirmed by the reference information: [1] expects it to be at 30.9 keV.

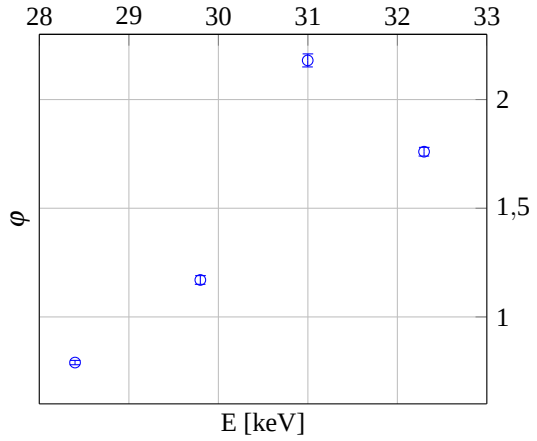

Fig. 1.20: ratio φ over the absorber's K edge energy [11]

conclusion

This experiment taught the qualities of both scintillation detectors and the germanium detector. The former is easier to use and requires less equipment, the latter retrieves data with a much better energy resolution. Both were actually used to gather data and had proven their abilities. The most outstanding problem is the multichannel analyser, more precisely, the definition of the count rate. The linear model the software relies on is not open to the user and seems unreliable since small changes in the peak's borders lead to dramatic changes for the values of gross and net area. Therefore a spectrum without any sources near to the detectors should be recorded and substracted from the measured data.

The spectra are distinct and most of the predicted effects could be observed. Moreover the analysis of the attenuation coefficient led to good coefficients of determination. One change to the setup seems reasonable: the duration of the measurement should be recorded by the computer. In this case the introduced error would be much smaller.

Literatur

[1] National Nuclear Data Center. Nudat 2.6. http://www.nndc.bnl.gov/nudat2/, 2012.

[2] W. Demtröder. *Experimentalphysik 4: Kern-, Teilchen- Und Astrophysik*. Springer, 2010.

[3] R. Erbrecht. *Das große Tafelwerk interaktiv*. Cornelsen, 2003.

[4] T. Friese. *Skript zur Vorlesung Nukleare Elektronik*.

[5] Detektor Systems GmbH. *Handbuch der Halbleiter für Nuklearstrahlung*. 1983.

[6] T. Möller J. Falta. *Forschung mit Synchrotronstrahlung*. Vieweg, 2010.

[7] B. Wiedemann K. Bethge, G. Walter. *Kernphysik: Eine Einführung*. Springer, 2008.

[8] G. Knoll. *Radiation Detection and Measurement*. Wiley, 2011.

[9] W. R. Leo. *Techniques for Nuclear and Particle Physics Experiments*. Springer.

[10] National Institute of Standards and Technology. X-ray mass attenuation coefficients. http://physics.nist.gov/PhysRefData/XrayMassCoef/tab3.html, 2012.

[11] National Institute of Standards and Technology. X-ray transition energies database. http://physics.nist.gov/PhysRefData/XrayTrans/Html/search.html, 2012.

[12] R. Szostak P. Marmier, E. Sheldon. *Kernphysik I*. Verlag der Fachvereine an der ETH Zürich, 1973.